Vibration-Temperature Separation Using Few-Mode Forward Transmission Distributed Fiber-Optic Sensor

Danxia Lu[®], Xing Rao[®], Shangwei Dai, Linqiao Du, Shen Liu[®], George Y. Chen[®], Senior Member, IEEE, and Yiping Wang[®], Senior Member, IEEE

Abstract—Long-distance distributed fiber-optic sensing can be achieved using forward transmission distributed sensing technology. However, current forward transmission methods struggle to distinguish between vibrations and temperature changes when their frequencies are similar, which poses a significant limitation for practical applications. We present and experimentally demonstrate a dual-parameter distributed sensing system based on forward transmission in a few-mode graded-index fiber, inphase/quadrature demodulation and phase-spectrum time delay methods to resolve the amplitude, frequency and position of vibrations. Simultaneous distributed sensing of vibration and temperature is demonstrated over 1 km of few-mode fiber, with vibration and temperature limit of detection as low as 26.1 p ε /Hz^{1/2} and 0.397 °C. The positioning results over sensing range of 2 km (without inline amplification) revealed that the positioning error can be as small as 0.2 m when employing bidirectional optical transmission (forward transmission). The vibration frequency range tested is between 100-600 Hz, limited by the piezoelectric transducer.

Received 21 November 2024; revised 19 March 2025 and 29 April 2025; accepted 14 June 2025. Date of publication 18 June 2025; date of current version 2 September 2025. This work was supported in part by the Ministry of Science and Technology of the People's Republic of China under Grant 2022YFE0111400, in part by the Scientific Instrument Developing Program of Shenzhen University under Grant 2023YQ027, in part by the Shenzhen Science and Technology Program (Shenzhen Key Laboratory of Ultrafast Laser Micro/Nano Manufacturing under Grant ZDSYS20220606100405013, in part by Shenzhen Science and Technology Program under Grant JCYJ20220818095800001 and Grant JCYJ20241202124408012, in part by the National Natural Science Foundation of China under Grant 62275172 and Grant U22A2088, and in part by the LingChuang Research Project of China National Nuclear Corporation. (Corresponding author: George Y. Chen.)

Danxia Lu, Xing Rao, Shangwei Dai, Linqiao Du, Shen Liu, and George Y. Chen are with the Shenzhen Key Laboratory of Photonic Devices and Sensing Systems for Internet of Things, Guangdong and Hong Kong Joint Research Centre for Optical Fibre Sensors, State Key Laboratory of Radio Frequency Heterogeneous Integration, Shenzhen University, Shenzhen 518060, China, and also with the Shenzhen Key Laboratory of Ultrafast Laser Micro/Nano Manufacturing, Key Laboratory of Optoelectronic Devices and Systems of Ministry of Education/Guangdong Province, College of Physics and Optoelectronic Engineering, Shenzhen University, Shenzhen 518060, China (e-mail: 2300453040 @email.szu.edu.cn; 2250453012@email.szu.edu.cn; daishangwei2023@email.szu.edu.cn; 2453232013@mails.szu.edu.cn; shenliu@szu.edu.cn; gychen@szu.edu.cn).

Yiping Wang is with the Shenzhen Key Laboratory of Photonic Devices and Sensing Systems for Internet of Things, Guangdong and Hong Kong Joint Research Centre for Optical Fibre Sensors, State Key Laboratory of Radio Frequency Heterogeneous Integration, Shenzhen University, Shenzhen 518060, China, also with the Shenzhen Key Laboratory of Ultrafast Laser Micro/Nano Manufacturing, Key Laboratory of Optoelectronic Devices and Systems of Ministry of Education/Guangdong Province, College of Physics and Optoelectronic Engineering, Shenzhen University, Shenzhen 518060, China, and also with the Guangdong Laboratory of Artificial Intelligence and Digital Economy (SZ), Shenzhen 518107, China (e-mail: ypwang@szu.edu.cn).

Color versions of one or more figures in this article are available at https://doi.org/10.1109/JLT.2025.3580762.

Digital Object Identifier 10.1109/JLT.2025.3580762

Index Terms—Distributed fiber-optic sensor, forward DAS, forward transmission, temperature measurement, vibration measurement.

I. INTRODUCTION

VER the past few decades, distributed fiber-optic sensing technology has made remarkable progress and has a wide range of applications in a variety of fields such as perimeter security protection, oil and gas pipeline leakage, intrusion monitoring, and seismic early warning [1], [2], [3]. Optical fiber is the core component of distributed fiber-optic sensors, being both the signal transmission medium and the sensing element to measure the physical parameters of the surrounding environment, such as temperature, pressure, strain and vibration. Temperature and vibration are among the most widely studied parameters.

In the majority of sensing systems, especially interferometric, changes in temperature and vibration can simultaneously affect the optical signal in the fiber, especially when they are of similar frequencies. Sensing mechanisms based on Raman scattering, Brillouin scattering or Rayleigh scattering from the pulsed transmission of optical signals have been extensively studied, including dual-parameter demodulation. One of the earliest proposed methods [4], that realized temperature-strain dual parametric sensing for the first time, experienced a drawback where differences in the environmental conditions and length differences between the sensing and reference fibers may lead lower measurement accuracy. A multi-parameter demodulation scheme based on a mixture of Brillouin frequency shift and the peak power was reported [5], but had limited spatial resolution due to power fluctuations in the measurements and random variations of the state of polarization. Researchers have also explored the use of photonic crystal fiber (PCF) [6], large-effective-area fiber (LEAF) [7], and polarization-maintaining fiber (PMF) [8] as sensing fibers for dual-parameter sensing, but the relatively small difference in Brillouin frequency constrains the temperature and strain accuracy. Hybrid Raman-Brillouin sensors [9] and hybrid Brillouin-Rayleigh sensors [10] were also considered as possible solutions to obtain higher spatial resolution and faster measurement time, but are setback by sensing distance limitation, which restricts their range of applications.

Forward transmission distributed sensing [10], [12], [13] is a promising class of sensor technology, though still in its infancy. It offers ultra-long-distance sensing due to the use of forward transmitted light instead of weak backscattered light. For instance, in the study by Yan et al [14], they proposed an

0733-8724 © 2025 IEEE. All rights reserved, including rights for text and data mining, and training of artificial intelligence and similar technologies. Personal use is permitted, but republication/redistribution requires IEEE permission. See https://www.ieee.org/publications/rights/index.html for more information.

ultra-long distance distributed vibration sensing system based on forward transmission and experimental results showed that spatial resolution of less than 125 m was achievable at a sensing distance of 615 km, which can cover a wide frequency range from infrasound to ultrasound. Shi et al [15] combined a bidirectionally pumped Raman fiber amplifier and a bi-directional EDFA to achieve 300 km relay-less long-distance sensing with a positioning error of less than 8 m. Rao et al. [16] reported 151.5 km single-span long-distance monitoring via a double-ended forward transmission and compensated self-interference mechanism. In addition, it potentially offers an unprecedented degree of communication-sensing deep integration [17]. However, this class of sensors are focused on efficient positioning of a single parameter (vibration) and lack the ability to distinguish between similar-frequency vibrations and temperature changes, which must be addressed for practical applications.

In recent years, few-mode fiber (FMF) [18], [19], [20], [21], [22] has become a research hotspot due to its ability to extend the transmission capacity of single-mode fiber (SMF) for space-division multiplexed optical communications. This also provides new opportunities for distributed fiber-optic sensing. FMF possess a larger modal area, which suppresses nonlinear effects and raises the damage threshold. FMF-based sensors also show great potential in realizing distributed multi-parameter measurements and ultra-long distance vibration sensing. In 2015, Li et al. [23] reported simultaneous temperature and strain measurements using the different SBS characteristics between LP₀₁ and LP₁₁ when using Brillouin optical time-domain analysis (BOTDA), solving the cross-sensitivity problem. In 2019, Fang et al. [24] demonstrated a Brillouin optical time-domain reflectometry (BOTDR) device based on elliptical-core FMF, and demonstrated simultaneous temperature and strain measurements. However, sensing systems based on Brillouin scattering are generally complex compared to Rayleigh scattering or forward transmitted light.

In this work, we propose a few-mode distributed vibrationtemperature dual-sensing system based on forward transmission. The system fundamentally relies on the weak coupling principle in FMF, where distinct spatial modes propagate with minimal inherent crosstalk unless perturbed by external measurands such as vibration or temperature variations. This principle, as demonstrated in prior works [25], [26], enables mode-specific responses to be isolated and analyzed, while perturbations induce quantifiable intermodal coupling through phase modulation. The concurrent measurement of vibration and temperature is realized by investigating the individual phase responses under different measurands and different modes. To the best of our knowledge, the proposed method has not been demonstrated for forward transmission distributed sensing. The sensor uses a two-mode graded-index FMF (2GI-FMF) as the sensing fiber, which has a relatively high nonlinear power threshold [27]. The graded-index profile can also help reduce differences in transit times between different modes, leading to a simpler positioning algorithm. A photonic-lantern-based mode multiplexer or demultiplexer is used at each detection end to ensure standard single-mode demodulation (retains phase delays from the FMF). In addition, in-phase/quadrature (IQ) demodulation technique

[28] and the double-ended phase-spectrum time delay method [29] are used to extract the phase information for analyzing the vibration amplitude, frequency and position along the FMF. The proposed sensing system is expected to achieve sensing distances up to hundreds of kilometers [29], [30] due to the use of forward-transmitting continuous-wave light instead of weak backscattered light.

II. OPERATION PRINCIPLE

In the proposed sensing system, phase modulation of the optical fiber represents changes in physical quantities (e.g., vibration, temperature, etc.). The use of interferometric techniques combined with phase demodulation algorithms can extract phase information from intensity variations. The phase of the optical signal is governed by the wavelength, fiber length and effective index, which can be expressed as:

$$\varphi = k_0 \, n_{eff} L \tag{1}$$

where φ is the phase delay, k_0 is the propagation constant of the light wave, n_{eff} is the effective refractive index of the mode, and L is the fiber length.

IQ coherent detection can be used to extract phase at each detection end. The continuous light wave is split into two beams of equal power by a 50/50 coupler. One beam is used as the reference arm, which is used as the local oscillator (LO) input of the 90° optical hybrid, while the other is the sensing arm, which is used as the sensing light (S) after phase modulated by vibration or temperature changes. Each of the two outputs of the optical hybrid is monitored by a balanced photodetector, and the alternative-current (AC) components of the photocurrents are:

$$I_{L}(t) = A_{L} A_{S} \cos \left[\varphi(t) + \varphi_{L} - \varphi_{S}\right] \tag{2}$$

$$I_Q(t) = A_L A_S \sin[\varphi(t) + \varphi_L - \varphi_S]$$
 (3)

where A_S and A_L are the amplitudes of the sensing signal and local-oscillator light, respectively, and $\varphi_L - \varphi_S$ is the phase difference between S and LO.

The phase could be demodulated as:

$$\varphi(t) = \arctan\left(\frac{I_Q(t)}{I_I(t)}\right)$$
 (4)

When a FMF is subjected to external factors such as vibration or temperature changes, the different transmitted modes are optically modulated by these changes. It has been found that for either vibration or temperature, its phase response coefficients of different modes of the FMF are not the same, which is key to solving the quadratic equation of phase shift resulting from two unknown measurands. This is likely attributed to the difference in modal area of each mode. On the other hand, the phase response to vibration and temperature are obviously not the same, and cannot be compared due to the different units. Strong perturbations such as significant bending (unlikely in a practical scenario where the optical fiber is protected in a cable) will change the geometry and refractive index distribution of the optical fiber, resulting in enhanced coupling between different modes, which can cause signal distortion, attenuation increase and vibration positioning inaccuracies [31]. While vibrations induce energy exchange (crosstalk) between modes, the coupling is typically not 100%. Each mode retains a portion of its independent phase evolution, allowing the demodulation process to resolve their individual phase contributions.

Since achieving vibration and temperature separation requires the combined phase shift to be measured across two separate modes, a mode-selective photonic lantern is used to facilitate the conversion of a fundamental mode to a higher order mode, and vice versa. Two modes with different vibration- and temperatureinduced phase responses are required, then discrimination can be achieved by computing a coefficient matrix [32]:

$$\begin{pmatrix} \Delta \varphi_1 \\ \Delta \varphi_2 \end{pmatrix} = \begin{pmatrix} C_{\varepsilon_1} & C_{T_1} \\ C_{\varepsilon_2} & C_{T_2} \end{pmatrix} \begin{pmatrix} \Delta \varepsilon \\ \Delta T \end{pmatrix} \tag{5}$$

where $\Delta \varphi_1$ and $\Delta \varphi_2$ represent the phase changes of LP₀₁ and LP_{11a}, respectively; $C_{\varepsilon 1}$, $C_{\varepsilon 2}$ and C_{T1} , C_{T2} are the vibration and temperature coefficients of LP₀₁ and LP_{11a}, respectively; and $\Delta \varepsilon$ and ΔT represent the changes in vibration and temperature, respectively.

If $C_{\varepsilon 1}C_{T2} \neq C_{\varepsilon 2}C_{T1}$, the measurands can be separate expressed as:

$$\begin{pmatrix} \Delta \varepsilon \\ \Delta T \end{pmatrix} = \frac{1}{|C_{\varepsilon 1} C_{T2} - C_{T1} C_{\varepsilon 2}|} \begin{pmatrix} C_{T2} & -C_{T1} \\ -C_{\varepsilon 2} & C_{\varepsilon 1} \end{pmatrix} \begin{pmatrix} \Delta \varphi_1 \\ \Delta \varphi_2 \end{pmatrix}$$
(6)

The differences in phase sensitivity between different modes in an optical fiber are mainly determined by the characteristics of their effective refractive indices, photoelasticity effects and mode field distributions. Specifically, due to the different effective indices of each mode, the same strain leads to different phase shifts. In addition, the photoelasticity effect indicates that the effective index change is proportional to the third power of the effective index. At the same time, spatial differences in the mode field distributions lead to different responses of the modes to strain-induced refractive index changes, such as bending or transverse strains. By taking into account the effective indices, the coefficients of thermal expansion, the thermo-optic coefficients, the elastic optical coefficients of the material, and the change in fiber length, it is possible to estimate the vibration and temperature sensitivity of the different modes. In theory, incorporating more modes into the optical fiber [33] can enhance the sensitivity via increasing the maximum effective index difference between the modes, but the average intermodal refractive difference is smaller, which leads to degenerate, strongly coupled modes (crosstalk) and increased modal dispersion. The increased mode coupling complicates signal processing, and thus raises the computation/hardware requirement.

III. EXPERIMENT SETUP

Fig. 1(a) shows the experiment setup of the single-ended detection system, which forms one end of the double-ended configuration needed for positioning. The output of an ultranarrow-linewidth CW tunable fiber laser (NKT E15 with 100 Hz linewidth) operating at 1550 nm was split into two branches by a 50/50 coupler. The lower branch is divided into two branches

by another 50/50 coupler to provide the LO inputs. The upper branch launched light into the fiber under test (FUT). A pair of photonic lanterns were used to selectively convert the fundamental mode of light into different modes of the FMF. Multiple connections allow the transmission of both LP_{01} and LP_{11} modes in 2GI-FMF. In order to test the phase response of the system under different vibrations (dynamic strain), 5 m of a FMF fiber was fixed around a 53 mm diameter disc-shaped piezoelectric transducer (PZT). An arbitrary waveform generator was used to produce a sinusoidal voltage signal to drive the PZT. A 1 km length of unstrained and unheated fiber was inserted after the PZT to separate the perturbed region from the 10 m of fiber placed in a temperature-controlled water bath (accuracy of ± 0.01 °C). At the FMF output, the modes are converted back to the fundamental mode via the corresponding ports of the photonic lantern. The phase delays experienced while propagating in the FMF are retained. Due to the graded-index profile, the optical path lengths between the different modes are approximately the same, allowing simpler demodulation. Subsequently, the single-mode light in different optical paths reach the detection end. Using single mode allows standard optical components and instruments to be employed, thus lowering the

At the detection end (both ends), the sensing optical signals are mixed with the two LO signals at the optical 90° hybrid, then four balanced photodetectors (10 MHz bandwidth) were used to convert the light intensity signals into voltage signals. The output signals from the BPDs were then digitally sampled by a real-time oscilloscope (1 GHz bandwidth). The sampling rate is configured at 1 kSa/s, limited by the system memory for long measurement durations, which is sufficient for low-frequency vibrations, and lowers the hardware requirement. However, it leads to a spectral aliasing due to the detection bandwidth (range of "signal" frequencies) being much larger than the sampling rate. The real-time oscilloscope collects data from two channels, representing the I component and the Q component. After which, the data of the two channels are divided by each other, then the phase data are obtained through the operations of arctan, phase unwrap and detrend. After obtaining the phase information, a Hann window FIR low-pass filter with a cutoff frequency of 10 Hz is performed to separate noise, and 1000-point moving averaging is used to further reduce noise. In the vibration analysis stage, the phase amplitude at different strains is obtained by Fast Fourier Transform (FFT) to deduce the linear relationship between phase and strain. In the temperature analysis stage, the data is downsampled to extract the phase value for each specific temperature point. The block diagram of data processing is shown in Fig. 1(c).

The sensing system shown in Fig. 1(b) is a folded double-ended detection configuration, which uses two modules of Fig. 1(a). The light from the same laser source is injected into both ends of the sensing fiber, and travels through the entire sensing fiber in both directions. When a perturbation occurs at a certain location, the wavefront of optical modulation arrives at the two detection ends at different times, which allows positioning via the phase-spectrum of fast Fourier transform.

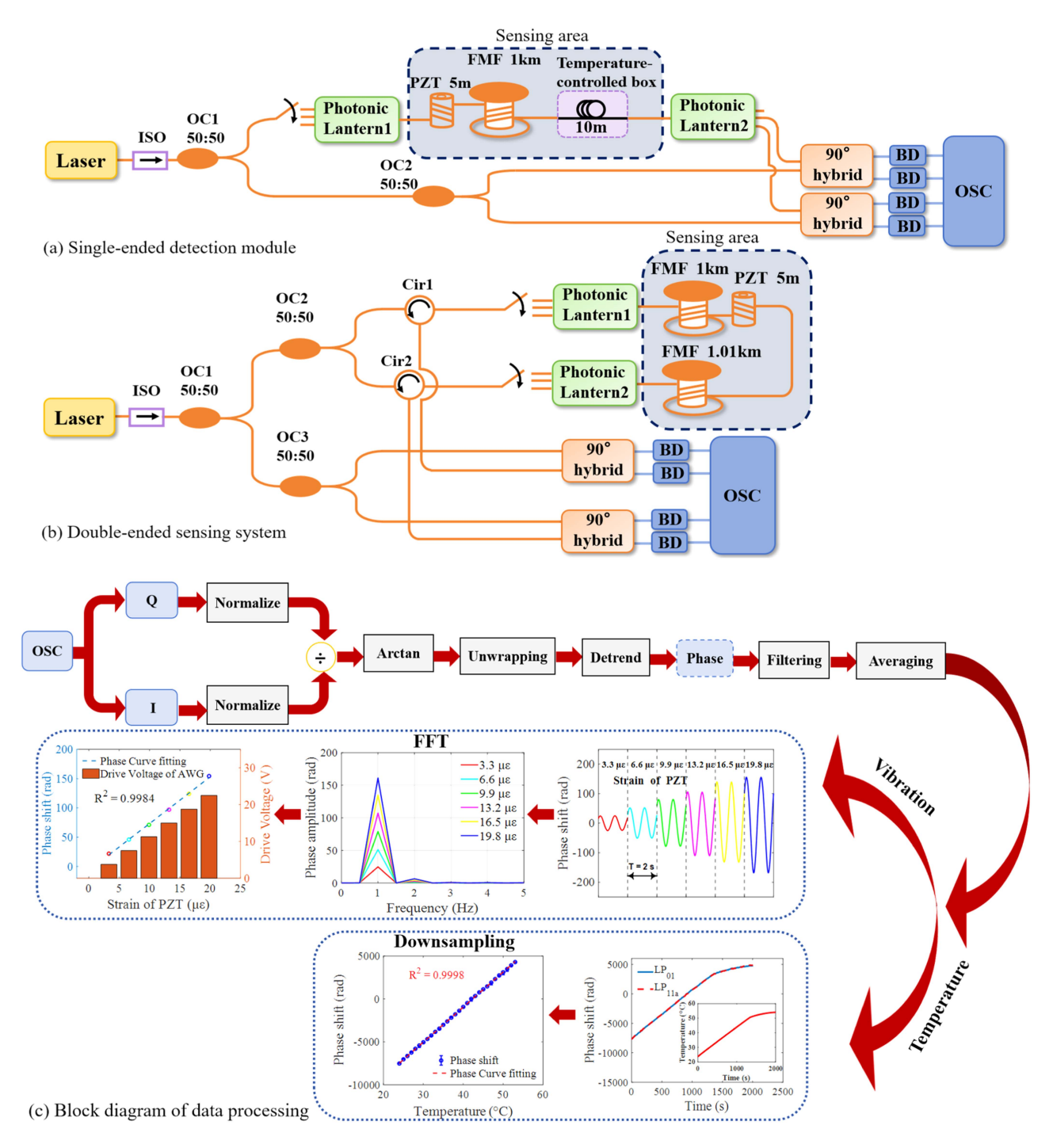


Fig. 1. Experiment setup: (a) Single-ended detection system, (b) Double-ended positioning system, (c) Block diagram of data processing (the "calibration" process to determine the sensitivity coefficients). ISO: Isolator, OC1, OC2: optic coupler, PZT: piezoelectric transducer, Cir1, Cir2: circulator, BPD: balance photodetector, OSC: Oscilloscope.

IV. RESULTS AND DISCUSSIONS

To evaluate the potential of the system for vibration and temperature measurements, and to assess the linearity of the system response, phase measurement experiments were carried out under different vibration and temperature conditions. The full details of the configurations used in the experiment are provided in experiment setup section. For temperature measurement, a single-point measurement was conducted by placing a 10 m length FMF in a temperature-regulated water bath, and incremented the temperature of water from 24 °C to 53 °C in steps of 1 °C, then measured the corresponding phase shift. As shown in Fig. 2, the trend of the phase shift changes as the temperature is gradually increased. For vibration measurement, the measurement of strain coefficients also involves quantifying

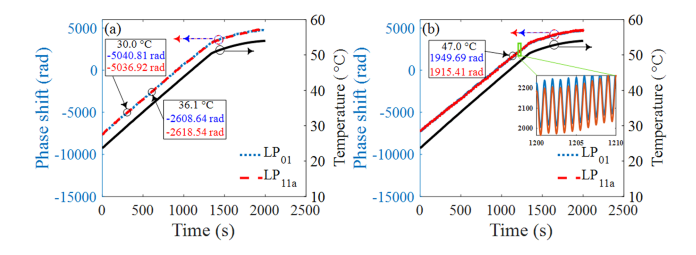


Fig. 2. Measured phase response: (a) Time-domain phase signal resulting from temperature changes, (b) Time-domain phase signal resulting from simultaneous temperature and vibration changes.

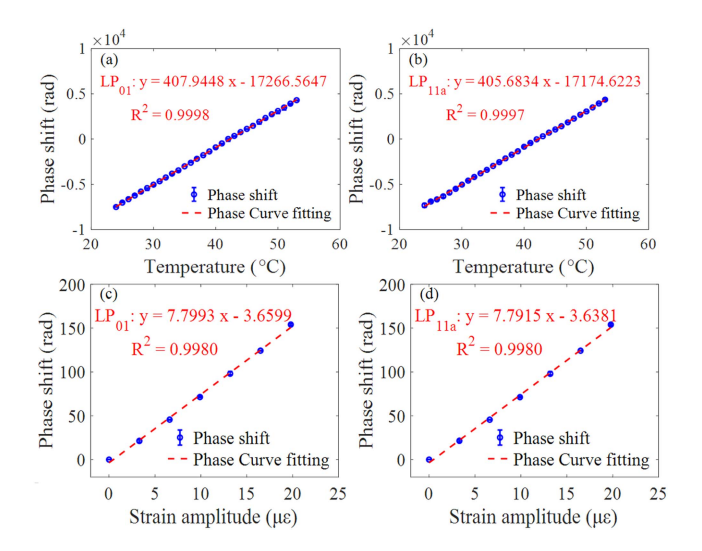


Fig. 3. Vibration (@ 1 Hz) and temperature sensitivity coefficients for different modes: (a) Temperature sensitivity of LP_{01} mode, (b) Temperature sensitivity of LP_{11a} mode, (c) Vibration sensitivity of LP_{01} mode, (d) Vibration sensitivity of LP_{11a} mode.

the phase response under different PZT strain conditions. For this characterization, the PZT was driven with sine signals of the same frequency but different amplitudes. Basically, the applied strain increased 0 $\mu\varepsilon$ to 19.8 $\mu\varepsilon$ with 3.3 $\mu\varepsilon$ per step. It was found that the phase difference gradually increased with increasing temperature or vibration. Since the effective refractive index difference between the LP01 and LP11a modes of the 2GI-FMF is relatively small, the phase shifts of the two modes are similar.

Fig. 3 shows the phase shift as a function of changing temperature or vibration (strain amplitude) for the LP₀₁ and LP_{11a} modes. By linear fitting the data, the temperature and vibration sensitivity are obtained. These are 407.9448 rad/°C and 7.7993 rad/ $\mu\varepsilon$ for LP₀₁ mode, and 405.6834 rad/°C and 7.7915 rad/ $\mu\varepsilon$ for LP_{11a} mode, respectively. It is evident that the two modes exhibit different sensitivities to temperature and vibration, making it possible to differentiate between them. The measured sensitivity coefficients of the two modes are used to validate the discrimination capability of the FMF-based forward transmission distributed sensor.

Phase noise data was collected over a duration of 10 ms in the absence of vibration, and the standard deviation (STD) was calculated. The inferred limit of detection (LoD) for temperature changes is 0.393 °C for LP₀₁ and 0.401 °C for LP_{11a}. Likewise,

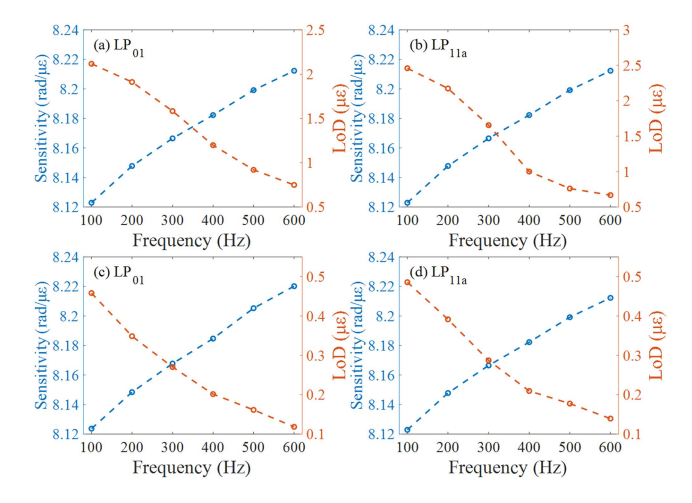


Fig. 4. Frequency response of sensitivity and limit of detection, based on the STD of noise: (a) LP_{01} mode, (b) LP_{11a} mode, based on the maximum noise amplitude using FFT: (c) LP_{01} mode, (d) LP_{11a} mode.

the vibration LoD (LoD = 3.3*std(phase noise)/sensitivity) is 2.3647 $\mu\varepsilon$ for LP₀₁ and 2.3923 $\mu\varepsilon$ for LP_{11a}. The normalized LoD is obtained by dividing the LoD by the square root of the detection bandwidth (10 MHz), yielding 747.78 p ε /Hz^{1/2} for LP₀₁ and 756.51 p ε /Hz^{1/2} for LP_{11a}.

The generic method (above) considers the noise contribution across all frequencies, which involves averaging (mean value) the standard deviations from 10 sets of phase noise data. An alternative method is proposed, which more accurately reflects the specific method. It involves performing a Fast Fourier Transform (FFT) on the phase noise data, then select the maximum noise amplitude within the frequency range of the vibration signals. Then, the average (mean value) of the 10 sets of phase noise data is obtained, and divided by the sensitivity to determine the LoD. The results of the second method give 26.1 p ε /Hz $^{1/2}$ for LP 11 and 28.2 p ε /Hz $^{1/2}$ for LP 11 a. As anticipated, the LoD calculated from the second method is lower. This is likely because only the noise components within a specific frequency range (i.e., that of vibrations) is considered.

For the practical test, the phase response of the sensor under the combination of vibration and temperature changes were recorded (see Fig. 2(b)). The temperature was varied from 30 °C to 47 °C, while the vibration-induced dynamic strain oscillated with an amplitude of 13.2 $\mu\varepsilon$ (previously calibrated using an interferometer). The measured phase shifts are 6990.50 and 6952.33 rad for the LP $_{01}$ and LP $_{11a}$ mode, respectively. By substituting the values into (6), the calculated vibration and temperature changes are $\Delta\varepsilon=15.61~\mu\varepsilon$ and $\Delta T=16.84$ °C. It can be seen that the difference between the measured values and the actual values are 2.41 $\mu\varepsilon$ and 0.16 °C. However, these values do not reflect the upper limit of the performance of the technique, and there is still a lot of potential for optimization.

Based on the differences in the sensitivity coefficients (phase shift) of the different modes of the few-mode fiber (FMF) to vibration and temperature, decoupling of vibration and temperature changes are realized by first measuring the phase-related sensitivity of different modes and constructing

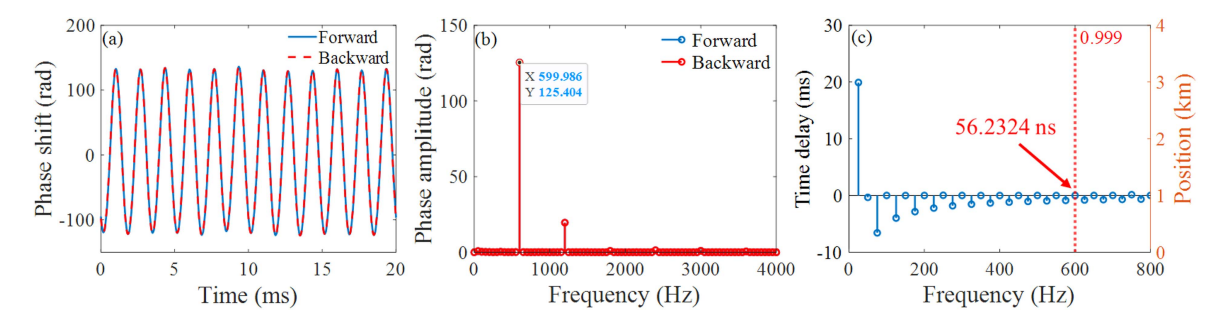


Fig. 5. Single-point vibration analysis @600 Hz: (a) Phase time-domain waveform, (b) Phase spectrum, (c) Time-delay spectrum.

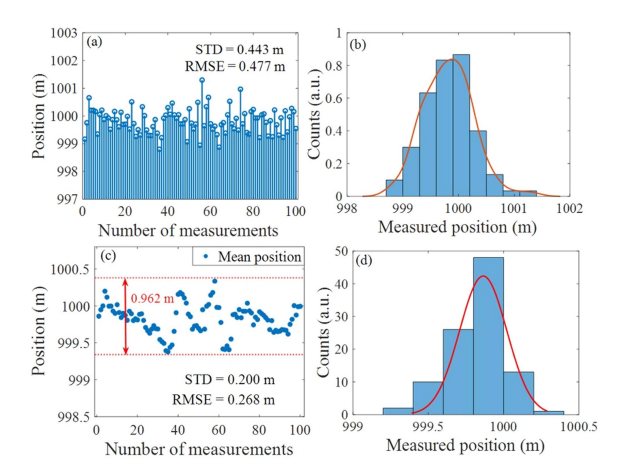


Fig. 6. Vibration positioning measurements: (a) Results of 100 consecutive positioning measurements, (b) Histogram of the distribution of measured positions, (c) Averaged results of 100 positioning measurements, (d) Histogram of the distribution of averaged positions.

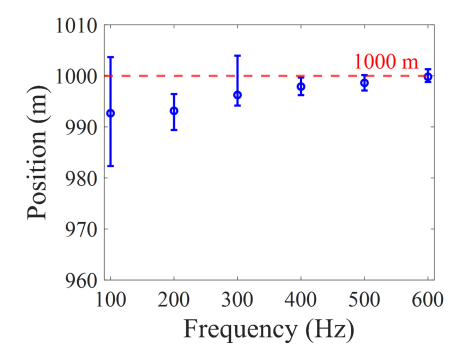


Fig. 7. System reliability characterization: Positioning accuracy as a function of vibration frequency.

a coefficient matrix, then solve the simultaneous equations of vibration/temperature involving the known coefficients and the measured phase values. However, the error in the actual measurement cannot be ignored. From the perspective of the experiment environment, the vibration amplitude was controlled at a specific value in the experiment, and the temperature fluctuate within a small range. Although the thermal enclosure used in the experiment mitigates to some extent the interference of the ambient temperature on the experiment results, it cannot completely isolate it. In addition, the photonic lantern may have defects such

as incomplete mode conversion and energy loss during the mode conversion process. The laser also exhibits long-term phase drift issues. All of these factors can affect the phase measurement accuracy.

In order to evaluate the frequency response of the sensing system, the drive voltage supplied to the PZT was varied and the demodulated phase shifts of the two modes, LP₀₁ and LP_{11a}, were analyzed. Subsequently, these data points were plotted with a linear fitting and the sensitivity was obtained from the gradient. As shown in Fig. 4, the study of the phase response under different PZT-induced vibration frequencies shows that the sensitivity increases and the LoD decreases with increasing vibration frequency. This may be due to the fact that higher-frequency vibrations may transfer strain with higher efficiency from the PZT to adhesive layer, then to the optical fiber, leading to greater phase shifts.

To evaluate the ability for distributed sensing and validate the positioning accuracy, the vibration source is located at the 1 km position (from nominal end of the sensing fiber), while the total length of the sensing fiber was extended to \sim 2 km. A vibration frequency of 600 Hz was applied to drive the PZT. The time-varying phase waveform is shown in Fig. 4, revealing a high degree of similarity between the forward and backward directions. Moreover, the observed time delay between the two detection ends is almost zero due to the position of the perturbation being close to the middle of the sensing fiber. From the phase spectrum plotted in Fig. 4(b), the 600 Hz signal is clearly detectable. Then, the phase-spectrum time delay method was employed to resolve the frequency components at each detection end, then calculate the difference between the initial phases, before finally converting the phase delay to a time delay and position. As depicted in Fig. 5(c), the time delay observed at the signal frequency of 600 Hz is 56.2324 ns. Utilizing the effective index of LP₀₁ at 1.446 and the speed of light in vacuum at 299792458 m/s, calculations reveal the vibration position should be at 999.167 m. This is in excellent agreement with the physically measured position at 1000 m.

A total of 100 consecutive vibration measurements were collected and analyzed for studying the repeatability, as presented in Fig. 6(a). Subsequently, Fig. 6(b) plots the histogram of the measurement results, showing the probability distribution of the measured vibration positions. The peak of the Gaussian fit curve is very close to 1000 m, consistent with the actual PZT position.

In order to evaluate the positioning accuracy of the system, the root mean square (RMS) error was calculated for 100 sets of data, and the result was 0.477 m. The mean value of position is 999.82 m. On the other hand, the standard deviation (STD) of multiple measurements is 0.443 m. It should be noted that the PZT is positioned at the mid-point of the sensing fiber, where the light in both directions travel a similar distance, resulting in similar changes in the state of polarization. Therefore, the interference results at the two detection ends are similar to waveform, leading to a relatively small positioning error. Subsequently, the 100 sets of positioning data were processed using a sliding 5-point mean filter, and the corresponding histogram of the averaged positioning values is plotted in Fig. 6(c) and (d). The calculated RMSE is 0.268 m, while the STD is 0.2 m.

To study the dependence of vibration positioning accuracy on the signal frequency, the frequency response was studied between 100-600 Hz. The characterization results are shown in Fig. 7, where it can be clearly seen that the positioning error decreases with increasing vibration frequency. This is because a higher frequency results in more signal cycles within the same measurement duration, leading to more accurate frequency estimation and positioning via the phase-spectrum time delay method. At a frequency of 100 Hz, the maximum standard deviation measured is 4.21 m. In contrast, the standard deviation of the positioning at 600 Hz is significantly smaller, at 0.443 m. This comparative result suggests complex vibration signals containing high-frequency components may facilitate higher positioning accuracy. Further observations indicate that at 600 Hz, the smallest deviation from the actual position of 1000 m is only 0.18 m.

V. CONCLUSION

A forward transmission distributed multi-parameter sensing system based on graded-index few-mode fiber (FMF) and phase demodulation was demonstrated to simultaneously measure vibration and temperature. This system uses forward transmitted continuous-wave light, which is known to yield higher intensity SNR and/or longer sensing distance. Although noise is integrated along the entire sensing fiber, which poses a problem for long-haul applications, vibration signals are also integrated and thus amplified. Moreover, signal processing algorithms such as variational mode decomposition can effectively extract signals from noisy sensor data. The FMF allows different phase response coefficients to distinguish different measurands. The graded-index profile minimizes modal dispersion, which simplifies positioning calculations. As a proof-of-concept demonstration, a 2 km length FMF was tested, with a positioning accuracy down to 0.2 m. The average vibration-phase sensitivity is 7.8 rad/ $\mu\varepsilon$ @ 1 Hz, corresponding to an LoD of 27.2 $p\varepsilon/Hz^{1/2}$. The average temperature-phase sensitivity is 406.81 rad/°C, corresponding to a resolution of 0.397 °C. The tested vibration frequency range was 100-600 Hz. Testing of actual simultaneous dual-parameter measurements revealed vibration and temperature deviations of 2.41 $\mu\varepsilon$ and 0.16 °C, respectively.

DISCLOSURES

The authors declare no conflicts of interest.

REFERENCES

- [1] J. M. Lopez-Higuera, L. Rodriguez Cobo, A. Q. Incera, and A. Cobo, "Fiber optic sensors in structural health monitoring," *J. Lightw. Technol.*, vol. 29, no. 4, pp. 587–608, Feb. 2011.
- [2] X. Li, Q. Sun, J. Wo, M. Zhang, and D. Liu, "Hybrid TDM/WDM-based fiber-optic sensor network for perimeter intrusion detection," *J. Lightw. Technol.*, vol. 30, no. 8, pp. 1113–1120, Apr. 2012.
- [3] G. Marra et al., "Ultrastable laser interferometry for earthquake detection with terrestrial and submarine," *Science*, vol. 361, no. 6401, pp. 486–496, Aug. 2018.
- [4] X. Bao et al., "Combined distributed temperature and strain sensor based on Brillouin loss in an optical fiber," Opt. Lett., vol. 19, no. 2, pp. 141–143, Ian. 1994
- [5] T. R. Parker et al., "Temperature and strain dependence of the power level and frequency of spontaneous Brillouin scattering in optical fibers," *Opt. Lett.*, vol. 22, no. 11, pp. 787–789, Jun. 1997.
- [6] L. F. Zou et al., "Brillouin scattering spectrum in photonic crystal fiber with a partially germanium-doped core," *Opt. Lett.*, vol. 28, no. 21, pp. 2022–2024, Nov. 2003.
- [7] X. Liu and X. Bao, "Brillouin spectrum in LEAF and simultaneous temperature and strain measurement," *J. Lightw. Technol.*, vol. 30, no. 8, pp. 1053–1059, Apr. 2012.
- [8] W. W. Zou et al., "Complete discrimination of strain and temperature using Brillouin frequency shift and birefringence in a polarization-maintaining fiber," Opt. Exp., vol. 17, no. 3, pp. 1248–1255, Feb. 2009.
- [9] M. Taki et al., "Hybrid Raman/Brillouin-optical-time-domain-analysis distributed optical fiber sensors based on cyclic pulse coding," *Opt. Lett.*, vol. 38, no. 20, pp. 4162–4165, Oct. 2013.
- [10] D. P. Zhou et al., "Distributed temperature and strain discrimination with stimulated Brillouin scattering and Rayleigh backscatter in an optical fiber," *Sensors*, vol. 13, no. 2, pp. 1836–1845, Jan. 2013.
- [11] Z. Zhan et al., "Optical polarization-based seismic and water wave sensing on transoceanic cables," *Science*, vol. 371, pp. 931–936, 2021.
- [12] Z. Sun, D. Huang, S. Li, H. Yang, and C. Zhao, "High-efficiency positioning of vibration intrusions for long-distance perimeter security monitoring based on time-frequency variation envelopes," *IEEE Trans. Instrum. Meas.*, vol. 73, 2024, Art. no. 3000711.
- [13] Z. Wu et al., "Long distance distributed optical fiber vibration sensing and positioning technology based on loop transmission polarization detection," *Measurement*, vol. 225, Dec. 2023, Art. no. 114029.
- [14] Y. Yan, F. N. Khan, B. Zhou, A. P. T. Lau, C. Lu, and C. Guo, "Forward transmission based ultra-long distributed vibration sensing with wide frequency response," *J. Lightw. Technol.*, vol. 39, no. 7, pp. 2241–2249, Apr. 2021.
- [15] F. Shi, R. Jin, Y. Du, C. Wang, and B. Jia, "Ultra-long-distance interferometric DOFS over 300 km without in-line repeater," *IEEE Photon. Technol. Lett.*, vol. 37, no. 5, pp. 289–292, Mar. 2025.
- [16] X. Rao, Y. Wang, M. Chen, K. Liu, G. Y. Chen, and Y. Wang, "150 km single-span distributed vibration sensor based on compensated self-interference forward transmission," *J. Lightw. Technol.*, vol. 42, no. 16, pp. 5736–5742, Aug. 2024.
- [17] R. L. Zhu et al., "Deep integration of fiber-optic communication and sensing systems using forward-transmission distributed vibration sensing and on-off keying," *Sensors*, vol. 24, 2024, Art. no. 5758.
- [18] A. Li et al., "Transmission of 107-Gb/s mode and polarization multiplexed CO-OFDM signal over a two-mode fiber," *Opt. Exp.*, vol. 19, no. 9, pp. 8808–8814, Apr. 2011.
- [19] A. Li, A. A. Amin, X. Chen, S. Chen, G. Gao, and W. Shieh, "Reception of dual-spatial-mode CO-OFDM signal over a two-mode fiber," *J. Lightw. Technol.*, vol. 30, no. 4, pp. 634–640, Feb. 2012.
- [20] C. Koebele et al., "Two mode transmission at 2×100 Gb/s, over 40 km-long prototype few-mode fiber, using LCOS-based programmable mode multiplexer and demultiplexer," *Opt. Exp.*, vol. 19, no. 17, pp. 16593–16600, Aug. 2011.
- [21] S. Randel et al., "6×56-Gb/s mode-division multiplexed transmission over 33-km few-mode fiber enabled by 6×6 MIMO equalization," *Opt. Exp.*, vol. 19, no. 17, pp. 16697–16707, Aug. 2011.
- [22] D. J. Richardson et al., "Space-division multiplexing in optical fibres," *Nature Photon.*, vol. 7, pp. 354–362, Apr. 2013.

- [23] A. Li et al., "Few-mode fiber based optical sensors," *Opt. Exp.*, vol. 23, pp. 1139–1150, Nov. 2015.
- [24] J. Fang et al., "Multi-parameter distributed fiber sensing with higher-order optical and acoustic modes," *Opt. Lett.*, vol. 44, no. 4, pp. 1096–1099, Feb. 2019.
- [25] L. Costa, Z. Zhan, and A. Marandi, "Mode-walk-off interferometry for position-resolved optical fiber sensing," *J. Lightw. Technol.*, vol. 41, no. 2, pp. 752–760, Jan. 2023.
- [26] J. Jia et al., "Distributed transverse stress sensor based on mode coupling in weakly-coupled FMF," *IEEE Photon. J.*, vol. 14, no. 1, Feb. 2022, Art. no. 6806706.
- [27] Y. Mao et al., "Investigating the performance of a few-mode fiber for distributed acoustic sensing," *IEEE Photon. J.*, vol. 11, no. 5, Oct. 2019, Art. no. 6802910.
- [28] Z. Wang et al., "Coherent Φ-OTDR based on I/Q demodulation and homodyne detection," Opt. Exp., vol. 24, no. 2, pp. 853–858, Jan. 2016.
- [29] X. Rao et al., "Multi-point vibration positioning method for long-distance forward transmission distributed vibration sensing," *Opt. Exp.*, vol. 32, pp. 30775–30786, 2024.
- [30] Z. F. Wu et al., "Long distance distributed optical fiber vibration sensing and positioning technology based on loop transmission polarization detection," *Measurement*, vol. 225, 2023, Art. no. 114029.
- [31] L. Palmieri, "Mode coupling in optical fibers," J. Lightw. Technol., vol. 43, no. 10, pp. 4995–5006, May 2025.
- [32] A. Li et al., "Few-mode fiber multi-parameter sensor with distributed temperature and strain discrimination," *Opt. Lett.*, vol. 40, no. 7, pp. 1488–1491, Mar. 2015.
- [33] L. Palmieri, "Coupling mechanism in multimode fibers," Proc. SPIE, vol. 9009, Feb. 2014, Art. no. 90090G.

Danxia Lu received the B.S. degree in light sources and lighting from Guangdong Polytechnic Normal University, Guangzhou, China, in 2023. She is currently working toward the M.S. degree with Shenzhen University, Shenzhen, China. Her research focuses on SDM distributed multi-parameter sensing based on phase-sensitive forward transmission of light.

Xing Rao received the B.S. degree in optoelectronic information science and engineering from Nanchang Hangkong University, Nanchang, China, in 2020. He is currently working toward the Ph.D. degree with Shenzhen University, Shenzhen, China. His research focuses on super long-range distributed vibration sensor based on polarimetric forward transmission of light.

Shangwei Dai received the master's degree in electronic information from Shantou University, Shantou, China, in 2023. He is currently working toward the Ph.D. degree with Shenzhen University, Shenzhen, China. His current research focuses on super long-range distributed vibration sensors based on phase-sensitive forward transmission of light.

Linqiao Du received the master's degree in electronic information from Henan Normal University, Henan, China, 2024. He is currently working toward the Ph.D. degree with Shenzhen University, Shenzhen, China. His current research focuses on super long-range distributed vibration sensor based on Raman amplification.

Shen Liu is currently the Deputy Director of Shenzhen Key Laboratory of Photonic Devices and Sensing Systems for Internet of Things. His research interests include fiber optic sensing technology, extreme environment mechanics sensing technology, fiber optic microcavity gas sensing technology, inertial devices and system applications; around the aerospace force thermal in-situ measurements and air and space inertial navigation core devices, to carry out fiber optic microcavity resonance device fabrication technology, sensing applications and system integration and other research. He was selected as one of Shenzhen's Outstanding Scientific and Technological Innovation Talents, Shenzhen's Overseas High-Level Talents, top 2% of the World's Top Scientists in the "Scientific Influence Ranking", and Shenzhen University's "Li-Yuan Excellent Young Scientists". He has been awarded with the nomination prize of the National Outstanding Doctoral Dissertation of Optical Engineering, Second Prize of the Ministry of Education's Natural Science Prize, and the First Prize of the Optics Science and Technology Prize of the Optical Society of Guangdong Province.

George Y. Chen (Senior Member, IEEE) received the 4-year M.Eng. (bachelor's and master's joint degree) in the field of electronics and electrical engineering with computer science from Imperial College London, London, U.K., in 2009, and the Ph.D. degree from the Optoelectronics Research Centre, University of Southampton, Southampton, U.K., in 2013. From 2013 to 2015, he was a Postdoctoral Research Fellow with Industrial Research Lab, SPI Lasers Ltd. He joined the University of South Australia, Adelaide, SA, Australia, as a Research Fellow in 2015, and a Senior Research Fellow in 2019. He was a part of the MinEx CRC. In 2021, he joined Shenzhen University, Shenzhen, China, as a Professor. He is a Senior Member of Optica.

Yiping Wang (Senior Member, IEEE) was born in Chongqing, China, in 1971. He received the B.Eng. degree in precision instrument engineering from the Xi'an Institute of Technology, Xi'an, China, in 1995, and the M.S. and Ph.D. degrees in optical engineering from Chongqing University, Chongqing, China, in 2000 and 2003, respectively. From 2003 to 2005, he was a Postdoctoral Fellow with Shanghai Jiao Tong University, Shanghai, China. From 2005 to 2007, he was a Postdoctoral Fellow with the Hong Kong Polytechnic University, Hong Kong. From 2007 to 2009, he was a Humboldt Research Fellow with the Institute of Photonic Technology, Jena, Germany. From 2009 to 2011, he was a Marie Curie Fellow with the Optoelectronics Research Centre, University of Southampton, Southampton, U.K. Since 2012, he has been a Distinguished Professor with Shenzhen University, Shenzhen, China. He has authored or coauthored one book, 21 patent applications, and more than 240 journal and conference papers. His research interests include optical fiber sensors, fiber gratings, and photonic crystal fibers. He is a Fellow of Optica.